https://doi.org/10.5194/acp-2019-1151
Preprint. Discussion started: 4 May 2020

Atmospheric Chemistry and Physics Discussions

Investigating three patterns of new particles growing to cloud condensation nuclei size in Beijing's urban atmosphere

Liya Ma[1], Yujiao Zhu[1, 2]*, Mei Zheng[3], Yele Sun[4], Lei Huang[1], Xiaohuan Liu[1], Yang Gao[1], Yanjie Shen[1], Huiwang Gao[1, 5] and Xiaohong Yao[1, 5]*

[1]Lab of Marine Environmental Science and Ecology, Ministry of Education, Ocean University of China, Qingdao 266100, China

[2]Environment Research Institute, Shandong University, Qingdao, Shandong 266237, China

[3]State Key Joint Laboratory for Environmental Simulation and Pollution Control, College of Environmental Sciences and Engineering, Peking University, Beijing 100871, China

[4]State Key Laboratory of Atmospheric Boundary Layer Physics and Atmospheric Chemistry, Institute of Atmospheric Physics, Chinese Academy of Sciences, Beijing 100029, China

[5]Laboratory for Marine Ecology and Environmental Sciences, Qingdao National Laboratory for Marine Science and Technology, Qingdao, China

Correspondence to: Xiaohong Yao and Yujiao Zhu (*xhyao@ouc.edu.cn, zhuyujiao@sdu.edu.cn)

Abstract. The growth of newly formed particles with diameters from ~10 nm to a larger size was investigated in Beijing's urban atmosphere on 10-23 December 2011, 12-27 April 2012 and through June-August 2014. The maximum geometric median diameter (D_{pgmax}) of newly formed particles in 11/27 new particle formation (NPF) events through June-August exceeded 75 nm, and the grown new particles may contribute to the population of cloud condensation nuclei. In contrast, no apparent growth in new particles with D_{pgmax}<20 nm was observed in all of the events occurring in December, in approximately half of the NPF events occurring in April and only 2/27 of the NPF events occurring in June-August. New particles observed in the latter NPF events were too small to be activated as cloud condensation nuclei. Apparent new particle growth with D_{pgmax}≤50 nm was observed in the remaining NPF events. The 11/27 NPF events with D_{pgmax} exceeded 75 nm were thereby analyzed in-depth. They are clearly three particle growth pattern classifications: one-stage growth, which is characterized by a continuous increase in D_{pgmax}≥80 nm (4/11 NPF events), and two-stage growth-A and growth-B, which are characterized by either no apparent growth (two-stage growth-A) or a shrinkage of particles (two-stage growth-B) in the middle 2-4 hours of the growth period (7/11 NPF events). Combining the observations of gaseous pollutants and the measured (or modeled) concentrations of particulate chemical species, the three growth patterns were discussed in terms of the spatial heterogeneity of NPF, the formation of secondary aerosols and the evaporation of semi-volatile particulates. Secondary organic species and NH_4NO_3 were argued to be two major contributors to the growth in new particles, but NH_4NO_3 likely contributed to growth only in the late afternoon and/or at nighttime.

1 Introduction

Atmospheric aerosol particles can be derived either from primary emissions, including various natural and anthropogenic sources, or from secondary sources (Yao et al., 2005; Sabaliauskas et al., 2012; Vu et al., 2015; Seinfeld and Pandis, 2016;

https://doi.org/10.5194/acp-2019-1151
Preprint. Discussion started: 4 May 2020

Atmospheric Chemistry and Physics Discussions

Quan et al., 2017; Zhu et al., 2019). Secondary sources are mainly related to atmospheric nucleation, followed by the growth in newly formed particles from ~1 nm to a larger size; this phenomenon is conventionally referred to as a new particle formation (NPF) event (Kulmala et al., 2004). In recent decades, thousands of studies on NPF have been reported, including field measurements in various atmospheres, laboratory studies on nucleation and the initial growth in newly formed particles, modeled NPF on a regional scale and its impacts on climate, new techniques developed for analyzing chemical components of nanoparticles and their gaseous precursors, etc. Building on these results, many review papers have summarized state-of-the-art progress and noted challenges for future works (Kulmala et al., 2004, 2012; Kulmala and Kerminen, 2008; Zhang et al., 2012, 2015; Kerminen et al., 2018; Chu et al., 2019; Lee et al., 2019).

Potential climate impacts of NPF events have been studied in the literature, e.g., 10% to 60% of NPF events have been reported to yield an appreciable contribution to cloud condensation nuclei (CCN) (Kuang et al., 2009; Asmi et al., 2011; Laakso et al., 2013; Yu et al., 2014; Rose et al., 2017; Kerminen et al., 2018). Modeled results have also proposed that approximately 50% of the CCN population is attributed to NPF events in the troposphere (Yu and Luo, 2009; Yu et al., 2014; Gordon et al., 2017). However, the reported observations have also shown that newly formed particles with diameters less than 40-50 nm can be activated as CCN only under high supersaturation (SS), e.g., >0.6% (Li et al., 2015; Ma et al., 2016). When newly formed particles grow with diameters greater than 70 nm, these new particles yield obvious contributions to the CCN population at SS=0.2% (Li et al., 2015; Zhu et al., 2019). In addition, field observations have also shown that the maximum diameter of grown new particles in most NPF events is less than 40-50 nm before new particle signals drop to a negligible level (Zhu et al., 2014, Liu et al., 2014; Man et al., 2015; Zhu et al., 2017; Yu et al., 2019). Thus far, which chemicals drive the growth in newly formed particles from ~10 nm to 40-70 nm remains poorly understood (Ehn et al., 2014; Chu et al., 2019; Lee et al., 2019).

In this paper, we studied observational data from three campaigns in Beijing. We focused on analyzing different growth patterns of newly formed particles with diameters from ~10 nm to a larger size, with particular attention to those NPF events in which the maximum diameter of grown new particles exceeded 70 nm. We combined the observations of gaseous pollutants and the observed (or modeled) concentrations of organic matter (or secondary organic aerosol, SOA), NO_3^- and NH_4^+, to interpret which chemicals drive the growth in new particles, e.g., varying major contributors in different growth periods. The survival probability ratios of newly formed particles, which can grow over 50 nm or 70 nm (two CCN threshold sizes under different SS), were also estimated. Our study provides new insight into the growth in newly formed particles to a larger size, as required for these particles to be activated as CCN at normal supersaturation in the atmosphere.

2 Methods

2.1 Sampling periods, sites and instruments

Two sampling sites were adopted to measure particle number concentration spectra in Beijing. Rooftop site is located on

https://doi.org/10.5194/acp-2019-1151
Preprint. Discussion started: 4 May 2020

the rooftop of an academic building inside the campus of Peking University (39.99°N, 116.31°E, ~20 m above ground level); Street site is a roadside site and is located approximately 200 m from rooftop site (Fig. 1). At rooftop site, the measurements were made on 16-23 December 2011, 12-27 April 2012 and 1 June - 31 August 2014. At street site, the measurements were made on 10-23 December 2011 and on 18-27 April 2012. The number concentrations of atmospheric particles were measured using a Fast Mobility Particle Sizer (FMPS, TSI Model 3091) downstream of a dryer (TSI, 3091) at a one second time resolution in each measurement campaign. The FMPS reported number size distributions of aerosol particles from 5.6 nm to 560 nm. Zimmerman (2015) proposed an empirical correction procedure for size distribution data reported by FMPS, which was then used for correction in this study. The scaling-down coefficient of the total particle number concentration measured by the FMPS (1.28) was obtained through a correlation analysis of the side-by-side measurements made by the FMPS and a condensation particle counter (CPC). A SO_2 analyzer (Thermo Model 43i), an O_3 analyzer (Thermo Model 49i), a NO_X analyzer (Thermo Model 42i) and a meteorological monitoring system were operated at a one-minute time resolution to obtain the real-time observational data of gases and meteorological parameters on the rooftop site close to the FMPS in 2011, 2012 and before 10 July in 2014. During the other observational periods, the mixing ratios of air pollutants at a one-hour time resolution and the meteorological data at a three-hour time resolution were taken from the Wanliu air quality monitoring station in Haidian district (39.99°N, 116.32°E, http://106.37.208.233:20035/) and the Beijing 54511 station (39.95°N, 116.30°E, https://rp5.ru/), respectively. The concentrations of organic matter (OM) as well as the inorganic species including NO_3^-, SO_4^{2-} and NH_4^+ in $PM_{1.0}$ during the period from 3 June to 11 July 2014 previously reported by Xu et al. (2017) were also used to facilitate the analysis. The data were measured by a High-Resolution Time-of-Flight AMS (HR-ToF-AMS) in 10 minutes time-resolution. The sampling site was located at a Tower branch of the Institute of Atmospheric Physics in Beijing, China (39.98°N, 116.38°E), and approximately 8 km away from Peking University.

2.2 Computational methods

NPF events were identified according to the definition by Dal Maso et al. (2005), and only NPF events with durations over one hour were analyzed in this study. In each NPF event, the net maximum increase in the nucleation mode particle number concentration (NMINP) was calculated according to Zhu et al. (2017). The nucleation mode was defined from 8 to 20 nm in this study.

$$NMINP = N_{8-20\ nm}(t_1) - N_{8-20\ nm}(t_0) \quad (1)$$

$N_{8-20\ nm}$ represents the sum of particle number concentrations with diameters from 8 nm to 20 nm, t_0 and t_1 represent the time of an NPF event to be initially observed and the time when the $N_{8-20\ nm}$ arrives at the maximum value, respectively.

The growth rate (GR) and shrinkage rate (SR) of new particles are determined by the slope of the fitted geometric median diameter of new particles (D_{pg}) with time (Whitby et al., 1978; Yao et al., 2010; Zhu et al., 2014; Man et al., 2015). In an NPF event or in each growth period of one NPF event, the maximum value of D_{pg} is defined as D_{pgmax}.

https://doi.org/10.5194/acp-2019-1151
Preprint. Discussion started: 4 May 2020

Atmospheric Chemistry and Physics Discussions

Lu et al. (2019) recently developed an equation to estimate the gaseous sulfuric acid concentration in Beijing. The equation is expressed as follows:

$$[H_2SO_4] = 280.05 \cdot UVB^{0.14} \cdot [SO_2]^{0.40} \quad (2)$$

The units for $[H_2SO_4]$ and $[SO_2]$ are molecule cm^{-3}, and the unit for UVB (ultraviolet B) is W m^{-2}. UVB occupies 5% of the ultraviolet radiation that reaches the Earth's surface (https://en.wikipedia.org/wiki/Ultraviolet#cite_note-Skin_Cancer_Foundation-23). Thus, UVB values were obtained by multiplying the downward ultraviolet radiation at the surface by 5% in this study, and the ultraviolet radiation was downloaded from https://cds.climate.copernicus.eu/. The contribution of sulfuric acid vapor to particle growth was calculated based on the method reported by Kulmala et al. (2001).

When D_{pg} of the grown new particles just reached 50 nm, the survival probability ratio (SPR) of grown new particles at D_{pg} = 50 nm was estimated as:

$$SPR = \frac{N_{50+3\sigma}}{NMINP} \times 100\% \quad (3)$$

where σ represents the standard deviation of the median diameter in the fitted log-normal distribution of grown new particles. $N_{50+3\sigma}$ refers to the integral value of the number concentration of new particles with the diameter from 50 nm to 50 + 3σ nm. We further defined another technical term, i.e., two times the SPR (2*SPR). The final SPR was between SPR and 2*SPR since some new particles with diameter from 50 - 3σ nm to 50 nm may eventually grow over 50 nm with an increase in D_{pg}. However, how many new particles with diameter from 50 - 3σ nm to 50 nm can grow over 50 nm varies case by case. The same can be said for the final SPR. Similar definitions are applied for the SPR of grown new particles with D_{pg} reaching over 70 nm.

The amount of chemical species required to grow new particles from D_{pg1} to D_{pg2} ($Mass_{requried}$) is roughly estimated as below (Man et al., 2015; Zhu et al., 2014):

$$Mass_{requried} = 4/3\pi\ [(D_{pg2}/2)^3 - (D_{pg1}/2)^3]*\bar{N}*\rho \quad (4)$$

$\bar{N}$ represents the average integral value of new particle number concentrations with the particle size from D_{pg1} to D_{pg2}; ρ is the density, which is assumed as 1.5 μg m^{-3} for SOA and 1.7 μg m^{-3} for NH_4NO_3, respectively. Local standard time was used to describe the NPF events in this paper.

2.3 Model description

U.S. EPA Community Multiscale Air Quality Model (CMAQ version5.0.2, Byun and Schere, 2006) was applied to simulate inorganic ions such as NO_3^-, SO_4^{2-}, NH_4^+ and SOA and total OM in $PM_{2.5}$ over East Asia. Fig. S1 shows the nested domains, with the 36 km domain 1 (d01) and the 12 km domain 2 (d02) over the eastern China and China adjacent seas. The vertical resolution includes 14 logarithmic structure layers from the surface to the tropopause, with the first model layer height of 36 m above the ground level. The meteorological fields were generated by the Weather Research and Forecasting (WRF) Model (v3.7). The input data for WRF were obtained from the National Center for Environmental Prediction (NCEP) Final

https://doi.org/10.5194/acp-2019-1151
Preprint. Discussion started: 4 May 2020

(FNL) Operational Global Analysis datasets (http://rda.ucar.edu/datasets/ds083.2). More detailed information about physical and chemical schemes used in meteorological simulations could be found in Zhang et al. (2019). Multi-resolution Emission Inventory for China (MEIC) in 2014 developed by Tsinghua University (http://www.meicmodel.org/) combined with BVOCs emissions generated from Gases and Aerosols from Nature (MEGAN v 2.0.4, Guenther et al., 2006) was used in this study. CB05tucl chemical mechanism module coupled with AERO6 was used to simulate concentrations of gases and aerosols. Initial conditions (ICONs) and boundary conditions (BCONs) of d01 were generated using the results from a global chemistry model of GEOS-Chem, while ICONs and BCONs for d02 are provided by results of d01. Five days spin-up time was used to minimize the influence of ICONs. Liu et al. (2010 a, b), Qi et al. (2018) and Zhang et al., (2019) reported the validation of the CMAQ application in China, in which good agreements between the simulated and measured concentrations of particulate components were generally obtained. Detailed evaluation results of this study could be found in Supporting Information.

3. Results

3.1 Overview of NPF events in three campaigns

A total of 46 NPF events were observed during three campaigns in Beijing, and the occurrence frequencies of NPF events decreased clearly in the rainy season (Table 1, Fig. S2). In Campaign 1, seven NPF events were observed on 10 - 23 December 2011 (7/14) at street site. On 16 - 23 December, three NPF events were observed (3/8) at rooftop site and occurred simultaneously with the events at the street site. In Campaign 2, seven NPF events were observed at rooftop site on 12-27 April 2012 (7/16). For measurements made at street site on 18-27 April 2012, two NPF events were observed simultaneously with the events observed (2/10) at the rooftop site. In Campaign 3, 13 NPF events occurred in June out of a total of 30 observational days. However, the occurrence frequency decreased to approximately 20% in July and August (seven NPF events from 31 observational days). Beijing enters the rainy season in July and August, and the weather conditions are unfavorable for NPF events (Wu et al., 2007).

The NMINP varied largely from event to event in the five months, but the monthly averages were generally closer to each other. For example, the monthly average values were $1.5\pm0.8\times10^4$ m^{-3} (average value ± standard deviation) in June 2014 and $1.6\pm0.8\times10^4$ m^{-3} in July and August 2014. The large values of NMINP implied the NPF to be an important source of ambient particles when particle number concentrations were considered. The NMINP was $1.6\pm0.7\times10^4$ m^{-3} at the rooftop site in April 2012, but it decreased to $1.3\pm0.2\times10^4$ m^{-3} at the street site. The NMINP at the rooftop site in December 2011 was only $8.3\pm4.2\times10^3$ m^{-3}, but it was still $1.5\pm0.7\times10^4$ m^{-3} at the street site. There was no significant difference in the NMINP at the rooftop site between April and June-August, but the values in the four months were significantly larger than those at the rooftop site in December ($P<0.05$). Zhu et al. (2017) discussed the seasonal difference in the NMINP between the two nearby sites in terms of the effects of the condensation sink and low temperature.

https://doi.org/10.5194/acp-2019-1151
Preprint. Discussion started: 4 May 2020

Atmospheric Chemistry and Physics Discussions

3.2 Season-dependent growth patterns of newly formed particles

When the growth behaviors of newly formed particles were studied, three growth patterns, i.e., Classes I, II and III, were identified (Figs. 2-4 and Figs. S3-6). Class I was characterized by no apparent particle growth. For example, the fitted D_{pg} of new particles was almost constant at 11 nm for ~10 hours on 25 April 2012 until the new particle signal dropped to a negligible level (Table 1, Fig. S3a). Class II was characterized by the fitted D_{pg} of new particles growing from 10±2 nm to 20-50 nm, e.g., in Fig. S3b-e. Class II can be further subclassified into four scenarios. In Scenario 1, the new particle growth lasted for a few hours with D_{pg} increasing to 27-48 nm and then stopping (Fig. S3b). The stop lasted for a few hours until the new particle signal dropped to a negligible level; in Scenario 2, new particles grew with D_{pg} approaching 32-45 nm. Afterwards, the signal of the new particles was apparently replaced by another signal of the new particles with an obviously smaller diameter (Fig. S3c). The phenomenon could also be explained by the spatial heterogeneity of NPF, as discussed later, and may not represent two NPF events occurring in one day. In Scenario 3, new particles grew with D_{pg} increasing to 20-50 nm, and the new particle signal was then overwhelmed by aged plumes. In the half or one hour transient period from new particle signals to aged plume signals, D_{pg} rapidly increased by dozens of nanometers (Fig. S3d), similar to those reported by Man et al. (2015). Scenarios 2 and 3 were associated with wind direction changes in the late afternoon or nighttime. Scenario 3 was quite common in the presence of air pollutant plumes (Levy et al., 2013; Zhang et al., 2015). In Scenario 4, the D_{pg} of new particles increased up to 31-50 nm. Afterwards, no data were available to judge any further particle growth (Fig. S3e). In Class III, the D_{pg} of new particles experienced either a continuous increase or a noncontinuous increase with the final D_{pgmax} closer to 75-120 nm (Figs. 2-4 and Figs. S4-6). Class III can be further classified into three growth patterns, which will be detailed later in this study. Overall, the D_{pgmax} of grown new particles increased from Class I to III.

In December, all of these observed NPF events (three NPF events at the rooftop site plus seven NPF events at the street site) were subject to Class I (Table 1, Fig. S2a). In April, 3/7 NPF events at the rooftop site and three NPF events simultaneously observed at the street site were subject to Class I. A total of 4/7 NPF events at the rooftop site in April were subject to Class II, of which half belonged to Scenarios 3 and 4 (Table 1, Fig. S2b). In June – August, a total of 2, 14 and 11 out of 27 NPF events were subject to Class I, Class II and Class III (Table 1, Fig. S2c-e), respectively. Newly formed particles in the summer appeared to have a high probability of growing to the CCN size, at least in 11/27 NPF events. On the other hand, newly formed particles in the winter unlikely acted as a potential source of CCN because of their D_{pgmax} only reaching 11±1 nm. However, the occurrence probability of Class I events largely decreased in the summer, i.e., no Class I NPF event in July and one Class I NPF event observed in each month of June and August (Table 1, Fig. S2c-e).

Overall, the growth patterns of newly formed particles are strongly season-dependent with the generally larger D_{pgmax} in June-August. The mechanisms for the growth in newly formed particles to the CCN size in Class III are thus critical for understanding the importance of grown new particles acting as a potential source of CCN at a normal supersaturation, such as

https://doi.org/10.5194/acp-2019-1151
Preprint. Discussion started: 4 May 2020

0.2%. The new particle growth behaviors in Class III NPF events were thus deeply studied, and the survival probabilities of the particles with D_{pgmax} at 50 nm and 70 nm are also estimated below.

3.3 Three growth patterns of newly formed particles reaching CCN size

When the observational results in June, July and August 2014 were examined separately, the occurrence frequencies of Class III NPF events in the three months were very close to each other, i.e., 4, 3 and 4 in June, July and August, respectively. The 11 NPF events can be further classified into three particle growth patterns, i.e., one-stage particle growth, two-stage particle growth-A and two-stage particle growth-B, as detailed below:

The one-stage particle growth pattern occurred in 4/11 NPF events, in which the fitted D_{pg} of newly formed particles continuously increased from 11 nm to 80-100 nm in 6-17 hours on 18 June, 12-13 July and 25 August 2014 (Fig. 2, Fig. S4). The new particle growth stopped at ~24:00 in 3/4 NPF events, while the new particle growth stopped as early as ~16:00 in the last event.

The two-stage particle growth-A pattern also included 4/11 NPF events, in which the D_{pg} of newly formed particles increased from 9-22 nm to 23-69 nm in the daytime, then oscillated for several hours, and eventually restarted the increase at nighttime (Fig. 3, Fig. S5). In 2/4 events, the D_{pg} of newly formed particles stopped the increase for 2~3 hours in the middle period and then restarted the increase up to 75 nm at 22:00. In the other 2/4 events, the D_{pg} stopped the increase for ~4 hours in the middle period and then restarted the increase up to 110-115 nm at 1:00 the next day.

A total of 3/11 NPF events experienced the two-stage particle growth-B, in which the D_{pg} of newly formed particles increased from 10-19 nm to 36-79 nm, then decreased down to 24-50 nm in the next 2-4 hours, and eventually restarted the increase with the D_{pg} up to 84-120 nm (Fig. 4, Fig. S6). In two events, the decrease in newly formed particles occurred at approximately 18:00, e.g., at 18:00-21:22 on 23 June and 17:50-20:30 on 26 July. However, the shrinkage occurred as early as 15:20-17:20 on 11 June.

4 Discussion

4.1 One-stage new particle growth to CCN size

Among four one-stage growth NPF events, newly formed particles took the shortest time to reach the maximum size on 18 June 2014 (Fig. 2a). The NPF event started to be observed at 09:20 and lasted for 11 hours. From 09:20 to 10:36, no apparent growth in newly formed particles was observed. The concentrations of gaseous precursors during that period may have been too low to cause a detectable growth in new particles with diameters >10 nm, similar to the observations reported in Hong Kong by Man et al. (2015). After 10:36, the D_{pg} of newly formed particles increased from 14 nm to 88 nm at 15:54 with a particle growth rate of 14 nm h^{-1}. The ambient relative humidity (RH) was approximately 40% with ambient temperature of approximately 30℃ (Fig. 2d), implying dry and hot conditions during the particle growth period. The observed mixing ratio

https://doi.org/10.5194/acp-2019-1151
Preprint. Discussion started: 4 May 2020

Atmospheric Chemistry and Physics Discussions

of O_x (NO_2+O_3) largely increased from ~ 60 ppb to ~ 130 ppb during the growth period, supporting the photochemical formation of secondary species to drive particle growth. Based on the observed mixing ratio of SO_2, sulfuric acid was estimated to contribute < 2% to the period particle growth (Fig. 2b). Wiedensohler et al. (2009), Ehn et al. (2014) and Wang et al. (2015) proposed that the photochemical formation of oxidized organic compounds played a more important role than the sulfuric acid vapor in growing new particles with diameters >10 nm in the daytime on basis of field measurements, laboratory experiments and modeling results. Assuming that the particle growth in this period was completely driven by secondary organic compounds, the required amount of SOA was estimated as 13 μg m^{-3}. The observed concentration of OM (including SOA and POA) in $PM_{1.0}$ increased by 15 μg m^{-3} during the five-hour growth period. The SOA seemingly acted as a major contributor to particle growth in this period, as supported by the decrease in the hygroscopicity parameter of 50 nm atmospheric particles from ~ 0.3 to ~ 0.1 during the same event independently reported by Wu et al. (2016). Almost constant concentrations of NO_3^- and NH_4^+ observed at 11:00-14:00, implied that no ammonium nitrate was freshly formed and contributed to the particle growth before 14:00 (Fig. 2c). From 14:00 to 16:00, the concentrations of NO_3^- and NH_4^+ largely increased. Assuming the increase in NO_3^- due to formation of NH_4NO_3, the net increase in NH_4NO_3 was 10 μg m^{-3}. Thus, formation of NH_4NO_3 may also play an important role in growing new particles after 14:00. Zhu et al. (2014) and Man et al (2015) reported that ammonium nitrate can be an important contributor to the growth in new particles (from 40-50 nm to a larger size at night). The new particles stopped growth after 15:54 until the new particle signal gradually disappeared at ~20:00. The observed concentrations of OM and NO_3^- had no increasing trends during the four hours, although they largely oscillated.

Another example subject to one-stage growth occurred on the event on 25 August 2014, and newly formed particles took the longest time to reach D_{pgmax} (Fig 3e). RH was lower than 50%, and the ambient air temperature varied from 24℃ to 31℃ during the growth period (Fig. 2h), also indicating dry and hot conditions during the particle growth period. The NPF event was observed from 07:50 on 25 August 2014 to 08:00 the next day (Fig. 2e). The new particle signal was unstable in the initial three hours due to the spatial heterogeneity of NPF.

The D_{pg} of newly formed particles started an increase from 12 nm at 10:48 to 80 nm at 24:00 with a particle growth rate of 5.1 nm h^{-1}. During the period of 11:00-19:00, sulfuric acid contributed to only 6% of the increase in D_{pg} from 12 nm to 51 nm on basis of the observed mixing ratios of SO_2. Because of the lack of photochemical reactions, nighttime sulfuric acid concentrations should have been much less than daytime sulfuric acid concentrations (Petäjä et al., 2009; Lu et al., 2019).

No measured concentrations of particulate chemical species were available on that day. Their modelled concentrations in $PM_{2.5}$ are alternatively used to argue possible contributors in growing newly formed particles, although the uncertainty may be even larger than the use of measured uparticulate species in $PM_{1.0}$. The modeled concentrations of SOA increased from 0.33 μg m^{-3} at 11:00 to 0.56 μg m^{-3} at 18:00 during the period (Fig. 2g), corresponding to an increase in D_{pg} of newly formed particles from 12 nm to 47 nm. Assuming that the particle growth was completely driven by the condensation of SOA, the

https://doi.org/10.5194/acp-2019-1151
Preprint. Discussion started: 4 May 2020

Atmospheric Chemistry and Physics Discussions

required amount of SOA was estimated to be 1.8 μg m^{-3}. The model evaluation in this study and previous studies show that the modeled concentrations of SOA are largely underestimated (see supporting information, Carlton et al., 2010; Hayes et al., 2015). Thus, the modeled concentrations of SOA were considered as a semiquantitative estimation to argue their contributions to growing new particles >10 nm. The modeled concentrations of NO_3^- and NH_4^+ were almost constant at 11:00-18:00 (Fig. 2g), suggesting that no NH_4NO_3 was newly formed to drive particle growth.

The modeled concentrations of SOA increased rapidly from 0.56 μg m^{-3} at 18:00 to 1.24 μg m^{-3} at 22:00 (Fig. 2g), with the D_{pg} of newly formed particles increasing from 47 nm to 70 nm. A total of 3.3 μg m^{-3} of SOA was required to drive the particle growth in this period if SOA were the only contributor. The modeled net increase in particulate ammonium nitrate was 3.6 μg m^{-3} from 18:00 to 22:00 (Fig. 2g). Assuming that the new particle growth from 18:00 to 22:00 was completely driven by ammonium nitrate, the required amount was estimated to be 3.8 μg m^{-3}. Ammonium nitrate may yield an important contribution to the particle growth in this period since its net increase apparently satisfied the required amount, to some extent. The D_{pg} of newly formed particles increased from 70 nm to ~80 nm from 22:00 to 24:00 when the modeled concentrations of all species decreased due to the dilution effect. Afterwards, the new particles stopped growing until their signal gradually disappeared at 08:00 the next day. The modeled concentrations of SOA and ammonium nitrate were almost constant after 1:00 the next day, consistent with the lack of apparent growth in these large new particles.

During the two NPF events on 12 and 13 July, sulfuric acid vapor was estimated as a minor contributor to particle growth (Fig. S4). The modeled results suggested that both ammonium nitrate and SOA were important contributors to particle growth, but ammonium nitrate contributed to growth only at nighttime (Fig. S4c, Fig. S4g). However, the concentrations of chemical species in different sized nanometer particles need to confirm this.

4.2 Two-stage new particle growth-A to CCN size

Fig. 3 and Fig. S5 show that the final D_{pgmax} of newly formed particles was 75 nm, 115 nm, 75 nm and 110 nm on 27 June, 6, 12 and 15 August 2014, respectively. On 27 June 2014 (Fig. 3a-d), the NPF events started to be observed at 09:00 and lasted for 18 h, with the RH generally lower than 40%. Apparent growth also cannot be observed for newly formed particles from 09:00 to 10:30. The D_{pg} of newly formed particles increased from ~10 nm at 10:30 to 35 nm at 15:20, with a GR of 5.2 nm h^{-1}. Using the observed mixing ratio of SO_2, sulfuric acid vapor was estimated to contribute 3% to the first stage particle growth (Fig. 3b). The constant concentrations of NO_3^- observed during the period implied that no ammonium nitrate was freshly formed and contributed to the period of particle growth (Fig. 3c). Assuming that the period particle growth was completely driven by SOA, the required amount of SOA was estimated as 0.64 μg m^{-3}. The observed OM dramatically varied at that period (Fig. 3c).

After 15:20, the D_{pg} of newly formed particles stopped the growth and fluctuated at approximately 35 nm for approximately two hours. The first stage particle growth apparently encountered an upper limit. Compared with the

https://doi.org/10.5194/acp-2019-1151
Preprint. Discussion started: 4 May 2020

concentrations observed before and after the two-hour period, the largely decreased number concentrations of newly formed particles implied spatial heterogeneity of NPF on that day, i.e., much weaker atmospheric nucleation generated newly formed particles in the upwind atmosphere at a certain spatial range, and the grown new particles at a lower number concentration were transported and observed at rooftop site at 15:20-17:40. The slightly decreased mixing ratios of O_x during this time, which were unexpected on the basis of a sharp increase in the observed O_x after the period, implying the reduced photochemical reaction activities in the upwind atmosphere at certain spatial ranges. The photochemical reaction activities during the period may be too weak to generate sufficient amounts of secondary organic and inorganic precursors in supporting the growth of new particles >35 nm to a larger size and subsequently lead to the growth encountering the upper limit, liking the diagram in the graph abstract.

After 17:40, the D_{pg} of newly formed particles started the second stage increase from 32 nm to 75 nm at 22:30, with a GR of 9.7 nm h^{-1}, which nearly doubled the growth rate observed during the first growth stage. The observed mixing ratio of O_x increased from 66 ppb at 17:20 to ~ 90 ppb at 21:20, supporting the secondary formation of chemical species to drive particle growth (Fig. 3b). The observed concentrations of OM and NO_3^- rapidly increased from 18:00 to 21:00 while the former was one order of magnitude larger than the latter. The required amount of NH_4NO_3 for the period particle growth was estimated as 4.0 μg m^{-3} while the net increase in NH_4NO_3 was 1.5 μg m^{-3}. SOA may dominate in growing new particles. Lee et al. (2016) and Huang et al. (2019) recently reported that the highly functionalized organonitrates (ON) generated from the reaction of NO_3 free radicals with organics can contribute to the growth in particles at nighttime. The observed concentrations of OM and NO_3^- largely oscillated and had no increasing trends after 21:00, although D_{pg} increased from 60 nm to 75 nm in one and half hours. After 22:30, the new particles stopped growing until their signal gradually disappeared at 03:00 the next day.

Following the analysis mentioned above, freshly formed SOA were argued to dominantly drive the first-stage particle growth on 6 August 2014 (Fig. 3e), on 12 and 15 August 2014 (Fig. S5). On the other hand, newly formed SOA and NH_4NO_3 were likely to be two major contributors to second-stage particle growth. Again, large uncertainties on modelled concentrations may exist due to lack of direct measurements of chemical species in different sized nanometer particles.

4.3 Two-stage new particle growth-B to CCN size

Among the three two-stage growth-B NPF events, the longest shrinkage in grown new particles occurred on 23 June 2014 (Fig. 4a) and lasted approximately 4 hours. On that day, our analysis implied the first stage particle growth to be driven by SOA. In detail, the D_{pg} of newly formed particles increased from 17 nm at 11:20 to 79 nm at 17:20, with a GR of 10 nm h^{-1}. From 11:20 to 17:20, the mixing ratio of O_x increased from 74 ppb to 122 ppb (Fig. 4b). A net increase in the observed OM was 14.6 μg m^{-3} during this period (Fig. 4c) while the required amount of SOA was estimated as 4.4 μg m^{-3}. SOA were very likely to be the major contributor to particle growth in this period. As independently reported by Wu et al. (2016), the hygroscopicity parameter of 50 nm atmospheric particles decreased from ~ 0.15 to ~ 0.05 during the same event. On the other

https://doi.org/10.5194/acp-2019-1151
Preprint. Discussion started: 4 May 2020

Atmospheric Chemistry and Physics Discussions

hand, the estimated sulfuric acid and observed NO_3^- plus NH_4^+ yielded either a small percentage or negligible contribution to particle growth in this period.

The D_{pg} of newly formed particles stopped growth at 79 nm from 17:20 through 18:00 and then decreased from 79 nm to 52 nm at 21:22, with a decreasing rate of 8 nm h^{-1}. During this period of shrinkage, the observed mixing ratio of O_x largely decreased from 130 ppb to 80 ppb (Fig. 4b). Repartition of the semivolatile species in gas and particle phases was hypothesized to cause the evaporation of semivolatile particulate species to the gas phase. Unfortunately, the observed OM fluctuated a lot at 20:00-22:00 when local signals of OM apparently overwhelmed its regional signals (Fig. 4c). The shrinkage may also be argued as spatial heterogeneity of NPF, but size-segregated number concentration modeling needs to confirm this.

After 21:22, the D_{pg} restarted to increase from ~50 nm to 90 nm over 4 hours. The formation of NH_4NO_3 likely yielded an important contribution to the second stage of particle growth, i.e., a net observed increase of 4.5 μg m^{-3} versus the required amount of 8.1 μg m^{-3}. SOA may also contribute to the second stage of particle growth on basis of a net increase in OM by 18 μg m^{-3} (Fig. 4c). After the second stage of growth, the D_{pg} of new particles experienced small oscillations at ~90 nm until the signal was overwhelmed completely by aged plumes.

Following a similar analysis on 23 June, reduced photochemical reaction activities were also argued to cause the shrinkage in newly formed particles on 11 June and 26 July 2014 (Fig. S6). The observed and modeled results for the two days implied that NH_4NO_3 played an important role in new particle growth only at night. In the daytime, SOA likely acted as the major contributor to particle growth.

4.4 Statistical analysis of factors related to new particle growth

The growth rate of newly formed particles is mainly determined by concentrations of condensable vapors such as sulfuric acid, organics in various volatilities, nitric acid and ammonia (Zhang et al., 2012; Ehn et al., 2014; Man et al., 2015; Lee et al., 2019). The D_{pgmax} are, however, determined by the total amount of vapors condensed on grown new particles, which may or may not have a positive correlation with the concentrations of these vapors (Zhu et al., 2019). When the values of D_{pgmax} are plotted against those of GR in Fig. 5a (two variables during the first growth period were used for plotting if two-stage particle growth existed), the values of D_{pgmax} largely scattered with r=0.23. When three circled points were excluded, the D_{pgmax} had a significant correlation with GR, but r value is still as low as 0.48 (Fig. 5a). GR alone is not sufficient to characterize the growth of newly formed particles by considering their potential impacts on the climate, and the D_{pgmax} and GR should be alternatively used.

As abovementioned, SOA and NH_4NO_3 are likely two major contributors to the new particle growth in different periods with the contributions of sulfuric acid only in a few percentages. Fig. 5b shows the net hourly increases in OM and NH_4NO_3 against the hourly required masses for particle growth by assuming the density of 1.5 μg m^{-3} for OM and 1.7 μg m^{-3} for NH_4NO_3. Both OM and NH_4NO_3 generally increase with increasing required masses and reasonably satisfy the required masses, but

https://doi.org/10.5194/acp-2019-1151
Preprint. Discussion started: 4 May 2020

Atmospheric Chemistry and Physics Discussions

they scatter largely in Fig. 5b. There is still a challenge to accurately quantify those contributors to the growth of newly formed particles.

The generation of OM and HNO_3 are strongly related to oxidation reactions at daytime. Thus, we further plot D_{pgmax} and GR against O_x (O_x=NO_2+O_3) during the particle growth period at daytime. Fig. 5c shows a good correlation between D_{pgmax} and O_x (the hourly average value when reaches D_{pgmax}) with r=0.80 and P<0.01. The slope further suggests that an increase of 10 ppb in O_x likely causes an increase of 5 nm in D_{pgmax}. The values of O_x in Class I NPF events were significantly smaller than those in Class II and Class II with P<0.05, and the lower O_x could be one of factors for no apparent particle growth in Class I. In addition, there was no significant difference of O_x between Class II and Class III. Including O_x, other factors should also affect the particle growth in Class I, II and III NPF events. Fig. 5d shows a significant correlation between GR and $\bar{O}_x$ (the average value during the whole growth period) with r=0.67 and P<0.01. The decreased r value implies the response of GR to the increase in O_x to be highly variable.

Oxidation products of biogenic VOCs, such as highly oxygenated molecules (HOMs), have been reportedly overwhelmed to determine the condensation growth of newly formed particles in the smaller size range because of their low volatilities (Ehn et al., 2014; Lee et al., 2019). In this study, the clear seasonal boundary of the Class I and Class II+III NPF events, e.g., 100% of Class I events in winter versus 7% and 93% of Class I and Class II+III events in summer, also points towards the importance of oxidation products of biogenic VOCs in growing particles from ~10 nm to larger size. In the summertime, theoretically increased emissions of biogenic VOCs and enhanced photochemical reactions indicating by O_x are expected to generate more HOMs for the growth of particles from ~10 nm to larger size. In spring, approximately half of NPF events are subject to Class I. However, there were no Class III then in. The seasonal transience may further imply that the generated amount of oxidation products of biogenic VOC not only determines the growth of new particles from ~10 nm to larger size, but also to CCN size. Unfortunately, we had no direct measurements of HOMs in small sized nanoparticles. In fact, it is still a common challenge to measure them for research community as reviewed by Lee et al (2019).

When the estimated CS were compared, the averaged value was $1.8\pm2.0\times10^{-2}$ s^{-1}, $2.1\pm1.5\times10^{-2}$ s^{-1} and $2.0\pm1.2\times10^{-2}$ s^{-1} for Class I, Class II and Class III, respectively. No significant difference exists between any two of them. Therefore, CS alone cannot explain the obtained three classes of particle growth patterns.

4.5 Final SPR during Class III NPF events

The potential contribution of new particles to the population CCN was evaluated by the calculated final SPR. In the Class III NPF events, final SPRs are listed in Table 1. For example, in the one-stage growth NPF event on 25 August 2014 (Fig. 2e), D_{pg} grew just beyond 50 nm at 19:00. At 19:46, the integral value of new particles larger than 50 nm increased to a maximum of 1.0×10^4 cm^{-3}. The maximum value of SPR_{50} was thus estimated as the final SPR, which was 42%. After 22:30, the D_{pg} reached only 70 nm. The integral value of grown new particles larger than 70 nm reached a maximum of 7.6×10^3 cm^{-3} at 24:00.

https://doi.org/10.5194/acp-2019-1151
Preprint. Discussion started: 4 May 2020

Atmospheric Chemistry and Physics Discussions

The final SPR_{70} was estimated as 32%. In the two-stage new particle growth on 27 June 2014 (Fig. 3a), the number concentrations of the integrated grown new particles larger than 50 nm reached a maximum value of 1.1×10^4 cm^{-3} at 21:32. The final SPR_{50} was thus estimated as 73%. The same method estimated that the final SPR_{70} was 49%, which also occurred at 21:32. Notably, the SPR was also influenced by NMINP, and a lower NMINP sometimes caused the larger SPR (e.g., 23 June, 12 and 15 August 2014). The final SPR values were even larger than 100% because of the spatial heterogeneity of NPF during NPF events. The uncertainty has also been reported in literature (Lihavainen et al., 2003; Rose et al., 2017, Lee et al., 2019), where the net contribution of NPF events to CCN was estimated.

Overall, in the Class III NPF events, the final SPR_{50} varied from 42% to 200%, with a median of 78%. Meanwhile, the final SPR_{70} varied from 31% to 138%, with a median of 57%. Our results implied that a significant fraction of new particles can grow to CCN size prior to being removed by atmospheric processes. Considering that high supersaturation sometimes occurred in the atmosphere (Fan et al., 2018), the new particles with D_{pg} increasing up to 50 nm may also be activated as CCN. Thus, > 40% of new particles in 11/27 NPF events in the summer of 2014 can reach 50 nm and may eventually contribute to the CCN population. When three growth patterns were analyzed separately, the final SPR_{50} and SPR_{70} varied from 42% to 78% and from 32% to 50%, respectively, in one-stage growth NPF events. The final SPR_{70} were significantly smaller than those of 49%-138% in two-stage growth-A plus growth-B NPF events with $P<0.05$. However, no significant difference of final SPR_{70} between two-stage growth-A and growth-B NPF events. A probably significant difference of SPR_{50} exists between in one-stage growth NPF events and two types of two-stage growth NPF events with $P=0.09$.

4.6 Spatial heterogeneity of NPF

The spatial heterogeneity of NPF can be clearly identified when high time-resolution measurements are made. Two NPF events were used as examples to demonstrate the spatial heterogeneity below.

On 6 August 2014 (Fig. 3e), the spatial heterogeneity of NPF clearly occurred and led to the signal of new particles largely dropping to a negligible level approximately one hour after 11:37 and then restarted to become detectable (Fig. 3e). The D_{pg} at approximately 17:40 jumped from 25 nm to 50 nm within five minutes, indicating a large spatial heterogeneity of NPF before and after 17:40-17:50. New particles observed after 17:51 were hypothesized to experience growth similar to the trend in the white dashed line (Fig. 3e) in the upwind atmosphere during the period from 11:37 to 17:51.

Moreover, both number concentrations and D_{pg} of new particles exhibited an inverted bell-shape at 23:00-01:51 on 6 August 2014 (Fig. 3e). The inverted bell-shape very likely reflected the spatial heterogeneity of NPF in the upwind atmosphere at a certain spatial range. The new particle signal was obviously enhanced after 01:51 on 7 August 2014. The new particles observed after the time were hypothesized to experience growth similar to the trend in white dashed line (Fig. 3e) in the upwind atmosphere.

The spatial heterogeneity of NPF was also obvious on 23 June (Fig. 4a). From 12:00 to 18:00, $N_{8\text{-}200nm}$ oscillated at

https://doi.org/10.5194/acp-2019-1151
Preprint. Discussion started: 4 May 2020

Atmospheric Chemistry and Physics Discussions

$1.2\pm0.2*10^4$ cm^{-3} (Fig. 4b). $N_{8\text{-}200nm}$ took approximately 20 minutes to increase to a higher level and then oscillated at $1.5\pm0.2*10^4$ cm^{-3} from 18:20 on 23 June to 01:30 on 24 June. $N_{8\text{-}200nm}$ then oscillated at $1.0\pm0.1*10^4$ cm^{-3} from 01:50 to 04:15 on 24 June.

Based on the time series of new particle number concentrations and their sizes observed, it can be inferred that the spatial heterogeneity of NPF occurred universally in each NPF event. This phenomenon should be considered for accurately evaluating the climate impacts of NPF events.

5 Conclusions

In this study, we investigated 46 NPF events in Beijing's urban atmosphere in three campaigns with particular attentions to the growth behaviors of newly formed particles. We first found that the maximum sizes of new particles grown were season dependent, e.g., D_{pgmax} can exceed 75 nm in 11 out of 27 NPF events only in summer, but no apparent growth in new particles with D_{pgmax} < 20 nm occurred in December across all events. Correlation analyses suggest that the concentrations of O_x may play an important role in determining D_{pgmax}, i.e., an increase of 10 ppb in O_x likely causes an increase of 5 nm in D_{pgmax}. The finding may allow us rethinking seasonal impacts of NPF events on the climate in Beijing and other urban areas in northern China.

According to the observed mixing ratio of SO_2, the sulfuric acid vapor generally yielded minor contributions to new particles growth. The observed and modeled concentrations of particulate chemical species suggested that the growth in newly formed particles in the daytime was mainly caused by OM/SOA. At night and late afternoon, the increased amount of NH_4NO_3 can reasonably account for the required amount to support new particle growth in most Class III NPF events. Besides, organics were also an important contributor to nighttime new particle growth in most Class III NPF events. However, direct measurements of these chemicals in different sized nanometer particles need to confirm this.

Regarding climates impacts of NPF events, the final SPR_{50} and final SPR_{70} are essential to be quantified. In Class III NPF events, the final SPR_{50} and final SPR_{70} varied from 42% to 200% and from 31% to 138%, respectively, implying that a significant fraction of new particles can grow to CCN size. However, the final SPR_{70} in one stage growth NPF events were significantly smaller than those of in two-stage growth-A plus growth-B NPF events with $P<0.05$. The difference is worthy of further investigation. However, no significant difference of final SPR_{70} between two-stage growth-A and growth-B NPF events. The percentage values of SPR_{50} and final SPR_{70} larger than 100% were due to spatial heterogeneity of NPF on a regional scale. The uncertainties on SPR_{50} and SPR_{70} associated with spatial heterogeneity of NPF cannot be removed on basis of observations alone while they may be reduced, to some extent, by a combination of observations and modeling results of newly formed particles in future. Our observations indicated that spatial heterogeneity always occurred in each NPF event to some extent and may be caused by varying photochemical reaction activities. When photochemical reaction activities are reduced, the growth in new particles can encounter an upper limit or experience a shrink in new particles. These factors should also be

https://doi.org/10.5194/acp-2019-1151
Preprint. Discussion started: 4 May 2020

Atmospheric Chemistry and Physics Discussions

considered for accurately evaluating the climate impacts of NPF events in the future.

Acknowledgment

This research is supported by the National Key Research and Development Program in China (grant no. 2016YFC0200504), the Natural Science Foundation of China (grant no. 41576118 and grant no. 41430646).

https://doi.org/10.5194/acp-2019-1151
Preprint. Discussion started: 4 May 2020

Atmospheric Chemistry and Physics Discussions

References

Asmi, E., Kivekäs, N., Kerminen, V.M., Komppula, M., Hyvärinen, A.P., Hatakka, J., Viisanen, Y., and Lihavainen, H.: Secondary new particle formation in Northern Finland Pallas site between the years 2000 and 2010, Atmos. Chem. Phys., 11, 12959-12972, doi: 10.5194/acp-11-12959-2011, 2011.

Byun, D and Schere, K.L.: Review of the Governing Equations, Computational Algorithms, and Other Components of the Models-3 Community Multiscale Air Quality (CMAQ) Modeling System. Applied Mechanics Reviews. 59, 51-77, doi: 10.1115/1.2128636, 2006.

Carlton, A.G., Bhave, P.V., Napelenok, S.L., Edney, E.O., Sarwar, G., Pinder, R.W., Pouliot, G.A., and Houyoux, M.: Model Representation of Secondary Organic Aerosol in CMAQv4.7, Environ. Sci. Technol., 44, 8553-8560, doi: 10.1021/es100636q, 2010.

Chu, B., Kerminen, V., Bianchi, F., Yan, C., Petäjä, T., and Kulmala, M.: Atmospheric new particle formation in China, Atmos. Chem. Phys., 19, 115-138, doi: 10.5194/acp-19-115-2019, 2019.

Dal Maso, M., Kulmala, M., Riipinen, I., Wagner, R., Hussein, T., Aalto, P.P., Lehtinen, K.E.J.: Formation and growth of fresh atmospheric aerosols: eight years of aerosol size distribution data from SMEAR II, Hyytiälä, Finland. Boreal Env. Res., 10, 323-336, doi: http://www.borenv.net/BER/pdfs/ber10/ber10-323.pdf, 2005.

Ehn, M., Thornton, J.A., Kleist, E., Sipilä, M., Junninen, H., Pullinen, I., Springer, M., Rubach, F., Tillmann, R., Lee, B., Lopez-Hilfiker, F., Andres, S., Acir, I., Rissanen, M., Jokinen, T., Schobesberger, S., Kangasluoma, J., Kontkanen, J., Nieminen, T., Kurtén, T., Nielsen, L.B., Jørgensen, S., Kjaergaard, H.G., Canagaratna, M., Maso, M.D., Berndt, T., Petäjä, T., Wahner, A., Kerminen, V., Kulmala, M., Worsnop, D.R., Wildt, J., and Mentel, T.F.: A large source of low-volatility secondary organic aerosol, Nature, 506, 476-479, doi: 10.1038/nature13032, 2014.

Fan, J., Rosenfeld, D., Zhang, Y., Giangrande, S.E., Li, Z., Machado, L.A.T., Martin, S.T., Yang,Y., Wang, J., Artaxo, P., Barbosa, H.M.J., Braga, R.C., Comstock, J.M., Feng, Z., Gao, W., Gomes, H.B., Mei, F., Pöhlker, C., Pöhlker, M.L., Pöschl, U., Souza, R.A.F.: Substantial convection and precipitation enhancements by ultrafine aerosol particles, Science, 359, 411-418. doi: http://science.sciencemag.org/, 2018.

Gordon, H., Kirkby, J., Baltensperger, U., Bianchi, F., Breitenlechner, M., Curtius, J., Dias, A., Dommen, J., Donahue, N.M., Dunne, E.M., Duplissy, J., Ehrhart, S., Flagan, R.C., Frege, C., Fuchs, C., Hansel, A., Hoyle, C.R., Kulmala, M., Kürten, A., Lehtipalo, K., Makhmutov, V., Molteni, U., Rissanen, M.P., Stozkhov, Y., Tröstl, J., Tsagkogeorgas, G., Wagner, R., Williamson, C., Wimmer, D., Winkler, P.M., Yan, C., and Carslaw, K.S.: Causes and importance of new particle formation in the present-day and preindustrial atmospheres, J. Geophys. Res. Atmos., 122, 8739-8760, doi: 10.1002/2017JD026844, 2017.

Guenther, A., Karl, T., Harley, P., Wiedinmyer, C., Palmer, P.I., Geron, C.: Estimates of global terrestrial isoprene emissions

https://doi.org/10.5194/acp-2019-1151
Preprint. Discussion started: 4 May 2020

using MEGAN (Model of Emissions of Gases and Aerosols from Nature), Atmos. Chem. Phys., 6, 3181-3210, doi: https://hal.archives-ouvertes.fr/hal-00295995, 2006.

Hayes, P.L., Carlton, A.G., Baker, K.R., Ahmadov, R., Washenfelder, R.A., Alvarez, S., Rappenglück, B., Gilman, J.B., Kuster, W.C., de Gouw, J.A., Zotter, P., Prévôt, A.S.H., Szidat, S., Kleindienst, T.E., Offenberg, J.H., Ma, P.K., and Jimenez, J.L.: Modeling the formation and aging of secondary organic aerosols in Los Angeles during CalNex 2010, Atmos. Chem. Phys., 15, 5773-5801, doi: 10.5194/acp-15-5773-2015, 2015.

Huang, W., Saathoff, H., Shen, X., Ramisetty, R., Leisner, T., and Mohr, C.: Chemical Characterization of Highly Functionalized Organonitrates Contributing to Night-Time Organic Aerosol Mass Loadings and Particle Growth, Environ. Sci. Technol., 53, 1165-1174, doi: 10.1021/acs.est.8b05826, 2019.

Kerminen, V., Chen, X., Vakkari, V., Petäjä, T., Kulmala, M., and Bianchi, F.: Atmospheric new particle formation and growth: review of field observations, Environ. Res. Lett., 13, 103003, doi: 10.1088/1748-9326/aadf3c, 2018.

Kuang, C., McMurry, P.H., and McCormick, A.V.: Determination of cloud condensation nuclei production from measured new particle formation events, Geophys. Res. Lett., 36, L09822, doi: 10.1029/2009GL037584, 2009.

Kulmala, M., Dal Maso, M., Mäkelä, J. M., Pirjola, L., Väkevä, M., Aalto P., Miikkulainen, P., Hämeri, K., O'dowd, C.D.: On the formation, growth and composition of nucleation mode particles, Tellus, 53B, 479–490, doi: org/10.1034/j.1600-0889.2001.530411.x, 2001.

Kulmala, M., Vehkamäki, H., Petäjä, T., Dal Maso, M., Lauri, A., Kerminen, V.M., Birmili, W., and McMurry, P.H.: Formation and growth rates of ultrafine atmospheric particles: a review of observations, J. Aerosol Sci., 35, 143-176, doi: 10.1016/j.jaerosci.2003.10.003, 2004.

Kulmala, M., and Kerminen, V.: On the formation and growth of atmospheric nanoparticles, Atmos. Res., 90, 132-150, doi: 10.1016/j.atmosres.2008.01.005, 2008.

Kulmala, M., Petäjä, T., Nieminen, T., Sipilä, M., Manninen, H. E., Lehtipalo, K., Dao Maso, M., Aalto, P. P., Junninen, H., Paasonen, P., Riipinen, I., Lehtinen, K. E. J., Laaksonen, A., and Kerminen, V-M.: Measurement of the nucleation of atmospheric aerosol particles, Nat. Protoc., 7, 1651–1667, doi: org/10.1038/nprot.2012.091, 2012.

Laakso, L., Merikanto, J., Vakkari, V., Laakso, H., Kulmala, M., Molefe, M., Kgabi, N., Mabaso, D., Carslaw, K.S., Spracklen, D.V., Lee, L.A., Reddington, C.L., and Kerminen, V.M.: Boundary layer nucleation as a source of new CCN in savannah environment, Atmos. Chem. Phys., 13, 1957-1972, doi: 10.5194/acp-13-1957-2013, 2013.

Lee, B.H., Mohr, C., Lopez-Hilfiker, F.D., Lutz, A., Hallquist, M., Lee, L., Romer, P., Cohen, R.C., Iyer, S., Kurtén, T., Hu, W., Day, D.A., Campuzano-Jost, P., Jimenez, J.L., Xu, L., Ng, N.L., Guo, H., Weber, R.J., Wild, R.J., Brown, S.S., Koss, A., de Gouw, J., Olson, K., Goldstein, A.H., Seco, R., Kim, S., McAvey, K., Shepson, P.B., Starn, T., Baumann, K., Edgerton, E.S., Liu, J., Shilling, J.E., Miller, D.O., Brune, W., Schobesberger, S., D'Ambro, E.L., and Thornton, J.A.: Highly

https://doi.org/10.5194/acp-2019-1151
Preprint. Discussion started: 4 May 2020

functionalized organic nitrates in the southeast United States: Contribution to secondary organic aerosol and reactive nitrogen budgets, P. Natl. Acad. Sci. USA., 113, 1516-1521, doi: 10.1073/pnas.1508108113, 2016.

Lee, S., Gordon, H., Yu, H., Lehtipalo, K., Haley, R., Li, Y., and Zhang, R.: New Particle Formation in the Atmosphere: From Molecular Clusters to Global Climate, J. Geophys. Res. Atmos., 124, 7098-7146, doi: 10.1029/2018JD029356, 2019.

Lihavainen, H., Kerminen, V.-M., Komppula, M., Hatakka, J., Aaltonen, V., Kulmala, M., and Viisanen, Y.: Production of "potential" cloud condensation nuclei associated with atmospheric new particle formation in northern Finland, J. Geophys. Res.-Atmos., 108, 4782, doi:10.1029/2003JD003887, 2003.

Levy, M.E., Zhang, R., Khalizov, A.F., Zheng, J., Collins, D.R., Glen, C.R., Wang, Y., Yu, X., Luke, W., Jayne, J.T., and Olaguer, E.: Measurements of submicron aerosols in Houston, Texas during the 2009 SHARP field campaign, J. Geophys. Res. Atmos., 118, 10, 518-10, 534, doi: 10.1002/jgrd.50785, 2013.

Li, J., Yin, Y., Li, P., Li, Z., Li, R., Cribb, M., Dong, Z., Zhang, F., Li, J., Ren, G., Jin, L., and Li, Y.: Aircraft measurements of the vertical distribution and activation property of aerosol particles over the Loess Plateau in China, Atmos. Res., 155, 73-86, doi: 10.1016/j.atmosres.2014.12.004, 2015.

Liu, X., Zhang, Y., Cheng, S., Xing, J., Zhang, Q., Streets, D.G., Jang, C., Wang, W., and Hao, J.: Understanding of regional air pollution over China using CMAQ, part I performance evaluation and seasonal variation, Atmos. Environ., 44, 2415-2426, doi: 10.1016/j.atmosenv.2010.03.035, 2010.

Liu, X., Zhang, Y., Xing, J., Zhang, Q., Wang, K., Streets, D.G., Jang, C., Wang, W., and Hao, J.: Understanding of regional air pollution over China using CMAQ, part II. Process analysis and sensitivity of ozone and particulate matter to precursor emissions, Atmos. Environ., 44, 3719-3727, doi: 10.1016/j.atmosenv.2010.03.036, 2010.

Liu, X.H., Zhu, Y.J., Zheng, M., Gao, H.W., and Yao, X.H.: Production and growth of new particles during two cruise campaigns in the marginal seas of China, Atmos. Chem. Phys., 14, 7941-7951, doi: 10.5194/acp-14-7941-2014, 2014.

Lu, Y., Yan, C., Fu, Y., Chen, Y., Liu, Y., Yang, G., Wang, Y., Bianchi, F., Chu, B., Zhou, Y., Yin, R., Baalbaki, R., Garmash, O., Deng, C., Wang, W., Liu, Y., Petäjä, T., Kerminen, V., Jiang, J., Kulmala, M., and Wang, L.: A proxy for atmospheric daytime gaseous sulfuric acid concentration in urban Beijing, Atmos. Chem. Phys., 19, 1971-1983, doi: 10.5194/acp-19-1971-2019, 2019.

Ma, N., Zhao, C., Tao, J., Wu, Z., Kecorius, S., Wang, Z., Größ, J., Liu, H., Bian, Y., Kuang, Y., Teich, M., Spindler, G., Müller, K., van Pinxteren, D., Herrmann, H., Hu, M., and Wiedensohler, A.: Variation of CCN activity during new particle formation events in the North China Plain, Atmos. Chem. Phys., 16, 8593-8607, doi: 10.5194/acp-16-8593-2016, 2016.

Man, H., Zhu, Y., Ji, F., Yao, X., Lau, N.T., Li, Y., Lee, B.P., and Chan, C.K.: Comparison of Daytime and Nighttime New Particle Growth at the HKUST Supersite in Hong Kong, Environ. Sci. Technol., 49, 7170-7178, doi: 10.1021/acs.est.5b02143, 2015.

https://doi.org/10.5194/acp-2019-1151
Preprint. Discussion started: 4 May 2020

Petäjä, T., Mauldin, R.L., Kosciuch, E., McGrath, J., Nieminen, T., Paasonen, P., Boy, M., Adamov, A., Kotiaho, T., Kulmala, M.: Sulfuric acid and OH concentrations in a boreal forest site, Atmos. Chem. Phys., 9, 7435–7448, doi: www.atmos-chem-phys.net/9/7435/2009/, 2009.

Qi, J., Liu, X., Yao, X., Zhang, R., Chen, X., Lin, X., Gao, H., and Liu, R.: The concentration, source and deposition flux of ammonium and nitrate in atmospheric particles during dust events at a coastal site in northern China, Atmos. Chem. Phys., 18, 571-586, doi: 10.5194/acp-18-571-2018, 2018.

Quan, J., Liu, Y., Liu, Q., Jia, X., Li, X., Gao, Y., Ding, D., Li, J., and Wang, Z.: Anthropogenic pollution elevates the peak height of new particle formation from planetary boundary layer to lower free troposphere, Geophys. Res. Lett., 44, 7537-7543, doi: 10.1002/2017GL074553, 2017.

Rose, C., Sellegri, K., Moreno, I., Velarde, F., Ramonet, M., Weinhold, K., Krejci, R., Andrade, M., Wiedensohler, A., Ginot, P., and Laj, P.: CCN production by new particle formation in the free troposphere, Atmos. Chem. Phys., 17, 1529-1541, doi: 10.5194/acp-17-1529-2017, 2017.

Sabaliauskas, K., Jeong, C., Yao, X., Jun, Y., Jadidian, P., and Evans, G.J.: Five-year roadside measurements of ultrafine particles in a major Canadian city, Atmos. Environ., 49, 245-256, doi: 10.1016/j.atmosenv.2011.11.052, 2012.

Seinfeld, J. I.: From Air Pollution to Climate Change, Environment: Science and Policy for Sustainable Development, Atmos. Chem. Phys., 40:7, 26-26, doi: 10.1080/00139157.1999.10544295, 1998.

Vu, T.V., Delgado-Saborit, J.M., and Harrison, R.M.: A review of hygroscopic growth factors of submicron aerosols from different sources and its implication for calculation of lung deposition efficiency of ambient aerosols, Air Qual. Atmos. Health., 8, 429-440, doi: 10.1007/s11869-015-0365-0, 2015.

Wang, Z.B., Hu, M., Pei, X.Y., Zhang, R.Y., Paasonen, P., Zheng, J., Yue, D.L., Wu, Z.J., Boy, M., and Wiedensohler, A.: Connection of organics to atmospheric new particle formation and growth at an urban site of Beijing, Atmos. Environ., 103, 7-17, doi:10.1016/j.atmosenv.2014.11.069, 2015.

Whitby, K. T.: The physical characteristics of sulfur aerosols, Atmos. Environ., 12(1-3), 135-159, https://doi.org/10.1016/B978-0-08-022932-4.50018-5, 1978.

Wiedensohler, A., Cheng, Y.F., Nowak, A., Wehner, B., Achtert, P., Berghof, M., Birmili, W., Wu Z.J., Hu, M., Zhu, T., Takegawa, N., Kita, K., Kondo, Y., Lou, S.R., Hofzumahaus, A., Holland, F., Wahner, A., Gunthe, S.S, Rose, D., Su, H., Pöschl, U.: Rapid aerosol particle growth and increase of cloud condensation nucleus activity by secondary aerosol formation and condensation: A case study for regional air pollution in northeastern china, J. Geophys. Res., 114, D00G08, doi: org/10.1029/2008JD010884, 2009.

Wu, Z., Hu, M., Liu, S., Wehner, B., Bauer, S., Ma ßling, A., Wiedensohler, A., Petäjä, T., Dal Maso, M., and Kulmala, M.: New particle formation in Beijing, China: Statistical analysis of a 1-year data set, J. Geophys. Res., 112, doi:

10.1029/2006JD007406, 2007.

Wu, Z.J., Zheng, J., Shang, D.J., Du, Z.F., Wu, Y.S., Zeng, L.M., Wiedensohler, A., and Hu, M.: Particle hygroscopicity and its link to chemical composition in the urban atmosphere of Beijing, China, during summertime, Atmos. Chem. Phys., 16, 1123-1138, doi: 10.5194/acp-16-1123-2016, 2016.

Xu, W.Q., Han, T.T., Du, W., Wang, Q.Q., Chen, C., Zhang, Y.J., Li, J., Fu, P.Q., Wang, Z.F., Worsnop, D.R., Sun, Y.L.: Effects of aqueous-phase and photochemical processing on secondary organic aerosol formation and evolution in Beijing, China, Environ. Sci. Technol., 51, 762-770, doi: 10.1021/acs.est.6b04498, 2017.

Yao, X., Choi, M.Y., Lau, N.T., Lau, A.P.S., Chan, C.K., and Fang, M.: Growth and Shrinkage of New Particles in the Atmosphere in Hong Kong, Aerosol Sci. Tech., 44, 639-650, doi: 10.1080/02786826.2010.482576, 2010.

Yao, X., Lau, N.T., Fang, M., and Chan, C.K.: Real-Time Observation of the Transformation of Ultrafine Atmospheric Particle Modes, Aerosol Sci. Tech., 39, 831-841, doi: 10.1080/02786820500295248, 2005.

Yu, F., Luo. G.: Simulation of particle size distribution with a global aerosol model: contribution of nucleation to aerosol and CCN number concentrations, Atmos. Chem. Phys., 9, 7691–7710, doi: www.atmos-chem-phys.net/9/7691/2009/, 2009.

Yu, F., and Hallar, A.G.: Difference in particle formation at a mountaintop location during spring and summer: Implications for the role of sulfuric acid and organics in nucleation, J. Geophys. Res. Atmos., 119, 12,246-12,255, doi: 10.1002/2014JD022136, 2014.

Yu, H., Ortega, J., Smith, J.N., Guenther, A.B., Kanawade, V.P., You, Y., Liu, Y., Hosman, K., Karl, T., Seco, R., Geron, C., Pallardy, S.G., Gu, L., Mikkilä, J., Lee, S.H.: New Particle Formation and Growth in an Isoprene-Dominated Ozark Forest: From Sub-5 nm to CCN-Active Sizes, Aerosol Sci. Technol., 48, 1285-1298, doi: www.tandfonline.com/loi/uast20, 2014.

Yu, H., Ren, L., Huang, X., Xie, M., He, J., and Xiao, H.: Iodine speciation and size distribution in ambient aerosols at a coastal new particle formation hotspot in China, Atmos. Chem. Phys., 19, 4025-4039, doi: 10.5194/acp-19-4025-2019, 2019.

Zhang, Q., Xue, D., Liu, X.H., Gong, X., Gao, H.W.: Process analysis of $PM_{2.5}$ pollution events in a coastal city of China using CMAQ, J. Environ. Sci. (China), 79, 225-238, doi: www.tandfonline.com/loi/uast20, 2019.

Zhang, R., Khalizov, A., Wang, L., Hu, M., and Xu, W.: Nucleation and Growth of Nanoparticles in the Atmosphere, Chem. Rev., 112, 1957-2011, doi: 10.1021/cr2001756, 2012.

Zhang, R., Wang, G., Guo, S., Zamora, M.L., Ying, Q., Lin, Y., Wang, W., Hu, M., and Wang, Y.: Formation of Urban Fine Particulate Matter, Chem. Rev., 115, 3803-3855, doi: 10.1021/acs.chemrev.5b00067, 2015.

Zhu, Y., Li, K., Shen, Y., Gao, Y., Liu, X., Yu, Y., Gao, H., and Yao, X.: New particle formation in the marine atmosphere during seven cruise campaigns, Atmos. Chem. Phys., 19, 89-113, doi: 10.5194/acp-19-89-2019, 2019.

Zhu, Y., Sabaliauskas, K., Liu, X., Meng, H., Gao, H., Jeong, C., Evans, G.J., and Yao, X.: Comparative analysis of new particle formation events in less and severely polluted urban atmosphere, Atmos. Environ., 98, 655-664, doi:

https://doi.org/10.5194/acp-2019-1151
Preprint. Discussion started: 4 May 2020

10.1016/j.atmosenv.2014.09.043, 2014.

Zhu, Y., Yan, C., Zhang, R., Wang, Z., Zheng, M., Gao, H., Gao, Y., and Yao, X.: Simultaneous measurements of new particle formation at 1 s time resolution at a street site and a rooftop site, Atmos. Chem. Phys., 17, 9469-9484, doi: 10.5194/acp-17-9469-2017, 2017.

Zimmerman, N., Jeong, C., Wang, J.M., Ramos, M., Wallace, J.S., and Evans, G.J.: A source-independent empirical correction procedure for the fast mobility and engine exhaust particle sizers, Atmos. Environ., 100, 178-184, doi: 10.1016/j.atmosenv.2014.10.054, 2015.

https://doi.org/10.5194/acp-2019-1151
Preprint. Discussion started: 4 May 2020

Atmospheric Chemistry and Physics Discussions

Abstract Art

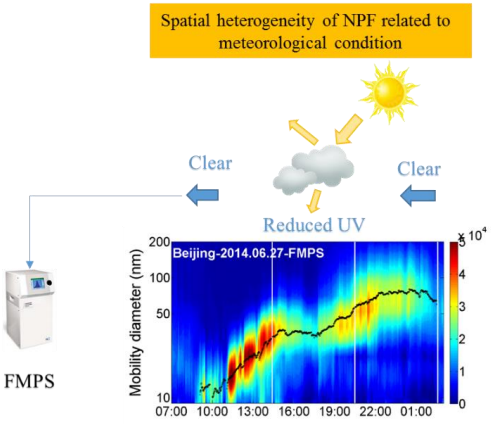

https://doi.org/10.5194/acp-2019-1151
Preprint. Discussion started: 4 May 2020

Atmospheric Chemistry and Physics Discussions

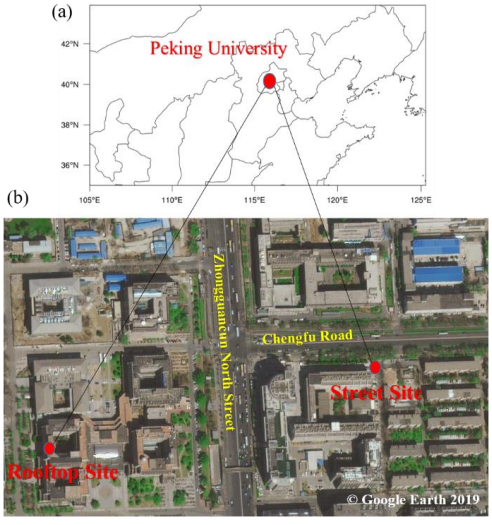

Fig. 1 Locations of the sampling sites (a) and satellite imagery of the two sampling sites (b) (downloaded from https://www.earthol.com/).

https://doi.org/10.5194/acp-2019-1151
Preprint. Discussion started: 4 May 2020

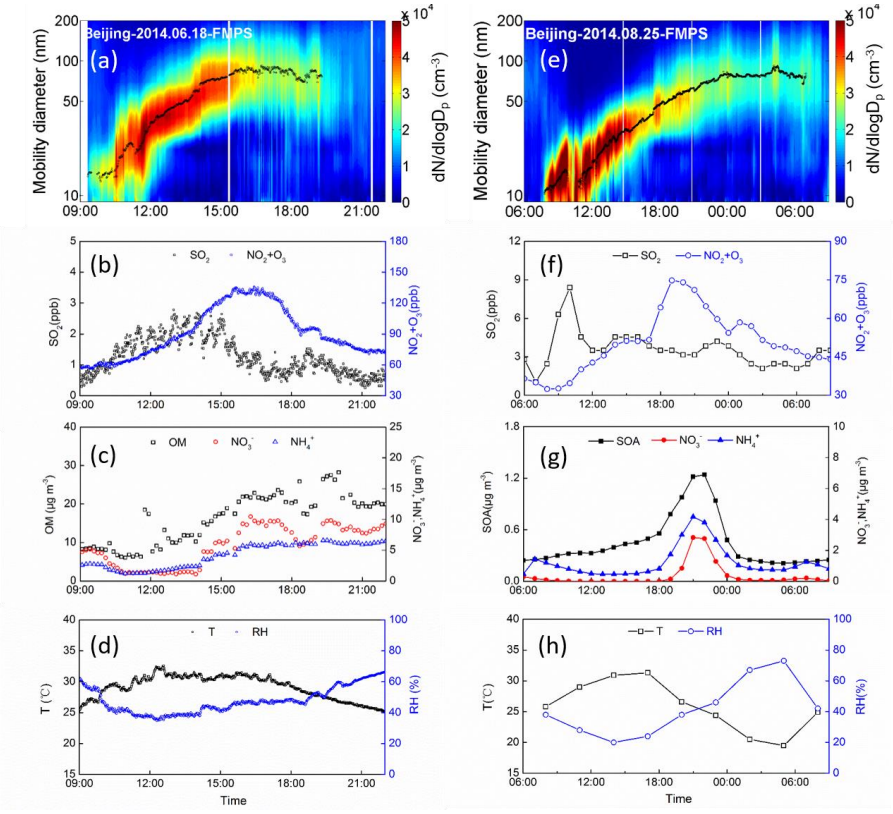

Fig. 2 NPF events occurred on 18 June and 25 August 2014 ((a, e) contour plot of the particle number concentration; (b, f) time series of the observed mixing ratios of SO_2 and NO_2+O_3; (c) time series of the observed OM, NO_3^- and NH_4^+ in $PM_{1.0}$; (d, h) time series of ambient T and RH; (g) time series of the modeled SOA, NO_3^- and NH_4^+ in $PM_{2.5}$).

https://doi.org/10.5194/acp-2019-1151
Preprint. Discussion started: 4 May 2020

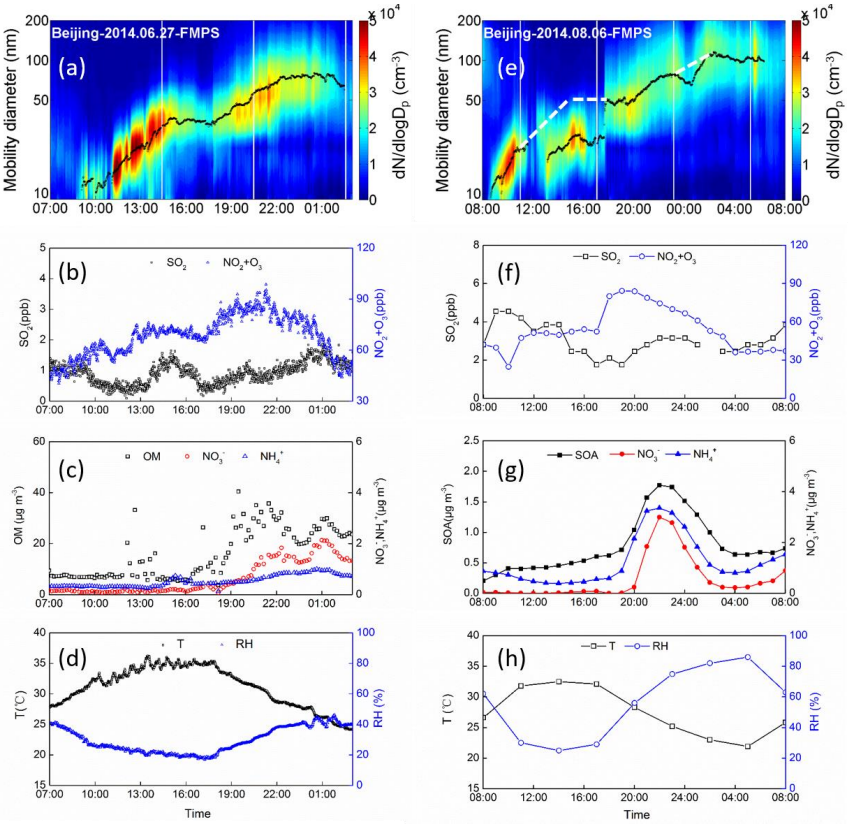

Fig. 3 NPF events occurred on 27 June and 6 August 2014 ((a, e) contour plot of the particle number concentration; (b, f) time series of the observed mixing ratios of SO_2 and NO_2+O_3; (c) time series of observed OM, NO_3^- and NH_4^+ in $PM_{1.0}$; (d, h) time series of ambient T and RH (g) time series of modeled SOA, NO_3^- and NH_4^+ in $PM_{2.5}$).

https://doi.org/10.5194/acp-2019-1151
Preprint. Discussion started: 4 May 2020

Atmospheric Chemistry and Physics Discussions

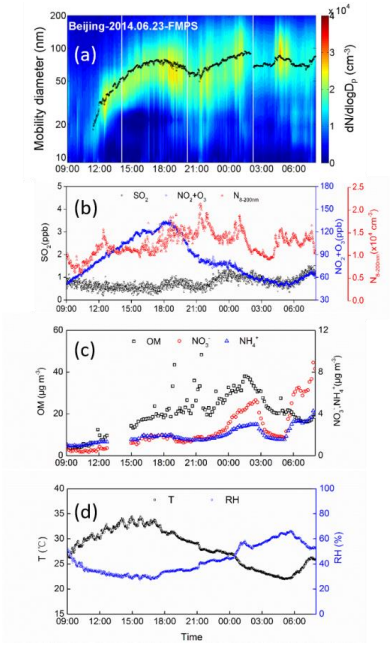

Fig. 4 NPF event that occurred on 23 June 2014 ((a) contour plot of the particle number concentration; (b) time series of the observed mixing ratios of SO_2, NO_2+O_3, and $N_{8\text{-}200\ nm}$; (c) time series of observed OM, NO_3^- and NH_4^+ in $PM_{1.0}$; (d) time series of ambient T and RH).

https://doi.org/10.5194/acp-2019-1151
Preprint. Discussion started: 4 May 2020

Atmospheric Chemistry and Physics Discussions

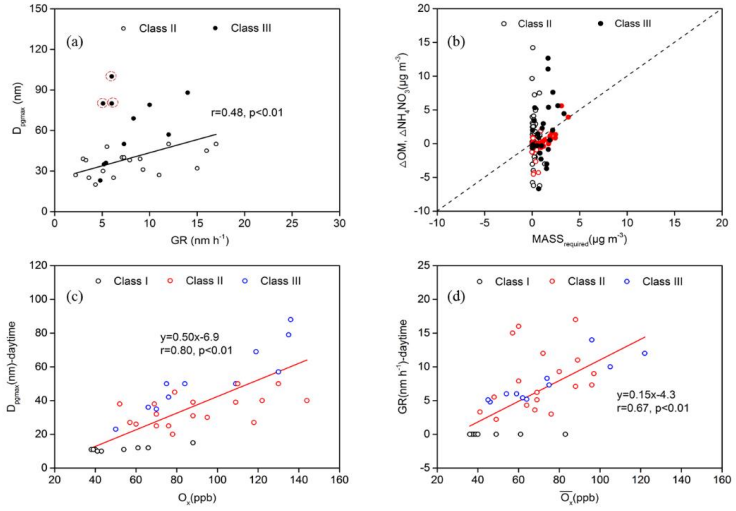

Fig. 5 Relationship between D_{pgmax} and GR (a); hourly variations in measured OM (black mark) and NH_4NO_3 (red mark, assuming NO_3^- to be completely associated with NH_4^+) versus required masses of OM and NH_4NO_3 for corresponding particle growth (b); relationship between D_{pgmax} in the daytime and the corresponding maximum O_x (c), and relationship between GRs in the daytime and the average mixing ratio of O_x (d).

https://doi.org/10.5194/acp-2019-1151
Preprint. Discussion started: 4 May 2020

Atmospheric Chemistry and Physics Discussions

Table1 Characteristics of NPF events in Beijing

Season	Date	Period	GR or SR ($nm\ h^{-1}$)	NMINP ($10^4 \#cm^{-3}$)	D_{pgmax} (nm)	SO_2 (ppb)[d]	SPR (%)	O_3+NO_2 (ppb)[f]
	10 Dec 2011*	9:00-15:00	-	1.5	11	2.5~4.4	-	36~38
	11 Dec 2011*	11:00-14:00	-	2.5	11	7.2~16	-	34~40
	14 Dec 2011*	10:00-16:00	-	1.1	11	3.1~5.8	-	31~39
	15 Dec 2011*	10:30-17:30	-	1.0	11	1.6~5.3	-	33~39
Winter	21 Dec 2011	13:00-18:00	-	0.5	10	1.4~3.5	-	33~43
	21 Dec 2011*	9:00-12:00	-	1.1	12	2.5~5.9	-	22~61
	22 Dec 2011	10:00-15:00	-	1.3	10	2.3~6.0	-	32~41
	22 Dec 2011*	11:30-15:40	-	2.3	10	2.3~7.6	-	23~41
	23 Dec 2011	11:00-14:00	-	0.7	10	3.5~16	-	32~43
	23 Dec 2011*	9:40-16:30	-	0.7	10	3.6~9.2	-	38~41
	12 Apr 2012	9:20-18:20	2.2	2.9	27	1.0~2.3	-	41~57
	13 Apr 2012	11:20-19:00	6.2	1.5	25	1.4~3.6	-	61~76
	14 Apr 2012	12:00-19:00	9.3	0.8	31	2.0~7.7	-	73~88
	15 Apr 2012	11:30-19:00	-	1.7	12	0.0~2.1	-	57~66
Spring	16 Apr 2012	10:22-14:20	7.9	1.2	38	1.3~3.7	-	52~69
	25 Apr 2012	10:07-20:00	-	1.0	11	0.0~1.9	-	47~54
	25 Apr 2012*	10:07-20:00	-	1.1	11	0.0~1.9	-	47~54
	27 Apr 2012	9:40-16:00	-	2.1	15	-	-	-
	27 Apr 2012*	9:40-16:00	-	1.4	15	-	-	-
	1 Jun 2014	12:00-16:00	-	1.1	15	0.4~1.5	-	77~88
	3 Jun 2014	8:00-12:00	4.3	3.0	20	1.2~10	-	56~78
	4 Jun 2014	11:30-22:00	11	1.2	27	1.2~3.7	-	67~118
	7 Jun 2014	9:00-(+1) 3:00	5.5	1.3	48	0.0~1.3	-	32~64
	8 Jun 2014	9:00-14:00	12	1.5	50	3.5~9.0	-	41~110
	9 Jun 2014	10:55-19:40	7.1	1.1	40	1.0~4.5	-	55~122
	11 Jun 2014	9:20-(+1) 3:20	5.4/5.1[a]/9.0[b]	1.1	36/84[c]	0.0~1.2	82/57[e]	43~89
	12 Jun 2014	8:00-15:00	3.6	3.1	25	1.2~7.3	-	50~87
	18 Jun 2014	9:20-20:20	14	1.8	88	0.4~2.8	78/50[e]	56~136
	23 Jun 2014	11:20-(+1) 1:22	10/8.0[a]/10[b]	0.5	79/90[c]	0.2~1.3	200/138[e]	53~135
Summer	27 Jun 2014	9:00-(+1) 3:00	5.2/9.7[b]	1.5	35/75[c]	0.1~1.9	73/49[e]	44~99
	28 Jun 2014	7:00-19:00	3.0	1.8	39	0.6~10	-	15~106
	29 Jun 2014	8:50-15:00	7.3	0.7	40	1.7~9.2	-	62~144
	8 Jul 2014	9:30-21:00	16	1.0	45	0.9~4.3	-	52~79
	9 Jul 2014	10:00-17:30	15	2.4	32	0.9~4.3	-	42~91
	12 Jul 2014	9:00-(+1) 4:00	6.0	1.6	80	1.8~3.5	66/43[e]	36~84
	13 Jul 2014	7:30-(+1) 4:00	6.0	2.5	100	2.1~5.6	56/31[e]	37~78
	14 Jul 2014	8:00-20:00	17	2.5	50	3.2~5.3	-	41~135
	25 Jul 2014	11:20-22:00	9.0	0.6	39	3.9~6.0	-	86~109
	26 Jul 2014	14:33-(+1) 8:00	12/8.2[a]/7.5[b]	0.9	57/120[c]	5.3~11	85/69[e]	23~130
	6 Aug 2014	8:41-(+1) 8:00	4.8/10[b]	1.4	23/115[c]	1.4~4.6	70/63[e]	25~82
	12 Aug 2014	10:00-22:00	7.3/6.5[b]	1.3	50/75[c]	2.1~4.6	106/65[e]	47~109
	15 Aug 2014	10:10-(+1) 3:42	8.3/8.7[b]	0.9	69/110[c]	2.1~6.3	156/121[e]	41~119

https://doi.org/10.5194/acp-2019-1151
Preprint. Discussion started: 4 May 2020

Atmospheric Chemistry and Physics Discussions

	24 Aug 2014	8:00-19:00	3.3	3.0	38	3.9~8.1	-	30~52
Summer	25 Aug 2014	7:50-(+1) 9:00	5.1	2.4	80	2.1~8.4	42/32[e]	32~75
	26 Aug 2014	9:00-23:00	5.1	1.1	30	0.7~7.0	-	44~95
	27 Aug 2014	12:25-14:30	-	1.1	12	-	-	-

*: The NPF events occurred on the street site.

[a]: Refers to the shrinkage rates of two-stage growth-B.

[b]: Refers to the second-stage growth rates.

[c]: Refers to the D_{pgmax} of the second-stage growth.

[d]: Refers to the mixing ratio range of SO_2 during the NPF period.

[e]: Refers to the SPR with the D_{pg} increasing up to 50 nm and 70 nm, respectively.

[f]: Refers to the mixing ratio range of O_x (NO_2+O_3) during the NPF period.